JOURNAL OF GUIDANCE, CONTROL, AND DYNAMICS
Vol. 26, No. 6, November–December 2003

Design Sensitivity Analysis for Helicopter Flight Dynamic and Aeromechanic Stability

Dario Fusato* and Roberto Celi†
University of Maryland, College Park, Maryland 20742-3015

An efficient technique is described to calculate the sensitivities of bandwidth and phase delay (defined according to the ADS-33 specification) and poles of a helicopter with respect to the blade torsion stiffness *GJ*. The technique is based on the derivation of expressions for the sensitivities using chain rule differentiation of appropriate portions of the equations of motion. Two configurations are studied, similar to the Eurocopter BO-105 and the Sikorsky UH-60. The study shows that the semi-analytical sensitivities are in excellent agreement with the corresponding finite difference-based sensitivities and that they are far less sensitive to step size. For the BO-105 configuration, phase bandwidth, gain bandwidth, phase delay, and poles are only weakly nonlinear functions of the torsion stiffness *GJ*, and therefore, linear approximations are accurate for broad variations of *GJ*. The same is mostly true for the UH-60 configuration, except that move limits are recommended for linear approximations to the phase delay at low *GJ*. The new technique is computationally very efficient. The additional cost of calculating the sensitivities is 4% of that of a complete linearized analysis, regardless of rotor configuration and flight speed. The figure is expected to apply also to sensitivities with respect to flap and lag stiffness.

Nomenclature

A	=	state matrix
A_{nr}	=	state matrix in nonrotating frame
B	=	control matrix
B_{nr}	=	control matrix in nonrotating frame
C	=	output matrix
D	=	distance from level 1 boundary in ADS-33 requirement charts
EI_2, EI_3	=	blade lag and flap bending stiffnesses
$G(i\omega)$	=	frequency-response matrix
GJ	=	blade torsion stiffness
M_t, M_l, M_f	=	elastic moment components acting on the blade section
p	=	generic design parameter
p, q, r	=	fuselage roll, pitch, and yaw rates
T	=	multiblade coordinate transformation matrix
$\boldsymbol{u}$	=	control vector
v, w, ϕ	=	blade elastic displacements
$\boldsymbol{x}$	=	state vector
$\boldsymbol{y}$	=	output vector
θ_G	=	geometric pitch angle of the cross section (pitch control angle plus builtin twist)
τ_p	=	time delay
ω_{BW}	=	bandwidth

Introduction

MODERN helicopters with advanced rotor and flight control systems can have unprecedented maneuverability and agility and increased mission effectiveness. However, their design has become more complex because it requires the careful integration of several disciplines. For example, model-following-type flight control systems can provide favorable, mission-tailored handling qualities, but can require high gains and reduce the aeromechanic stability margin of some key rotor modes. Conversely, low damping of rotor modes can result in long transients and vibrations during aggressive maneuvers, with negative repercussions on handling qualities; these problems cannot easily be solved through feedback control.

A multidisciplinary approach requires the analysis of the mutual interactions among a variety of design parameters, from different disciplines. These analyses can be quite complex, and improved mathematical tools are necessary to make them manageable. As the number of design parameters increases, it becomes more and more time consuming to perform systematic parametric studies. Similarly, as the interactions among different disciplines in new more advanced designs increase, so does the number of designers from each discipline who need to communicate and attempt to share their intuitions and experience to solve the multidisciplinary problems. Formal sensitivity analysis and optimization techniques can effectively support the multidisciplinary design process because they can deal with multiple design parameters and multidisciplinary problems in an efficient and systematic way.

The present paper describes a portion of the development of a design-oriented helicopter flight dynamic simulation program.[1] The words design oriented denote an analysis that generates, in a single pass and with a small additional computational cost, not only the behavior quantities of interest, but also their derivatives (or sensitivities) with respect to a series of parameters. The behavior quantities addressed by the present paper are the bandwidth and phase delay as defined by the ADS-33 handling qualities specification.[2]

The derivatives of interest could be calculated numerically, using finite differences. This technique is very easy to implement, but is computationally expensive: The derivatives with respect to n parameters require $n+1$ or $2n+1$ function evaluations if one-sided or central differences are used, respectively. Furthermore, an appropriate finite difference step size needs to be determined: The derivatives can be inaccurate because of cancellation and truncation errors if the step sizes are too small or too large, respectively.

An alternative technique consists of obtaining analytical derivatives,[3] by obtaining expressions for the derivatives of interest through chain rule differentiation of the governing equations. Often the most computationally expensive portions of the resulting expressions are already available from the baseline calculations and can be reused at no additional cost. Other portions can be inexpensively calculated using finite differences (in which case the derivatives are called semi-analytical). In this case, the additional cost for the derivatives can be a small fraction of that of the baseline analysis.

Received 28 October 2002; revision received 13 June 2003; accepted for publication 16 June 2003.

*Ph.D. Candidate, Department of Aerospace Engineering, Alfred Gessow Rotorcraft Center.

†Professor, Department of Aerospace Engineering, Alfred Gessow Rotorcraft Center. Member AIAA.

With the partial exception of Ref. 4, little or no information is available in the literature on analytical or semi-analytical sensitivity calculations of quantities of interest in handling qualities calculations, such as bandwidth and phase delay, with respect to rotor and fuselage design parameters. In Ref. 4, the derivation of approximate gradients of the quantities required to evaluate compliance with the quickness criteria of ADS-33 is described, but the approximations are obtained through a simplified frequency-domain model and not from the chain rule differentiation of the governing equations.

A multidisciplinary rotor–flight control system optimization study, with aeroelastic and handling qualities constraints, is described in Ref. 5. However, in this study, the gradients of objective function and constraints were all calculated using finite difference approximations, and the simulation model was rather simple. Analytical or semi-analytical gradients have been obtained for other quantities of interest in rotorcraft engineering. Because their primary focus is aerodynamics and aeroelasticity, these studies will not be summarized here. A review of such work may be found in Ref. 6.

In light of the preceding discussion, the main objective of the present paper is to present in detail a methodology for efficient calculations of sensitivities of the frequency response of a helicopter to pilot inputs and of its open-loop poles with respect to rotor design parameters. The torsion stiffness of the rotor blades is used as the specific design variable, and quantitative results are presented, which include comparisons of the sensitivities obtained with the new method and those obtained with traditional finite difference-based techniques.

As already mentioned, a design-oriented analysis provides both behavior quantities and sensitivities information for an additional cost that is just a small portion of the entire analysis. The design-oriented analysis can either be used in isolation or inserted in a design optimization loop. The most powerful optimization algorithms require the gradients of the objective functions and the constraints with respect to the design variables. Therefore, efficient sensitivity calculations are a key factor in reducing the computational requirements of the optimization. For optimization-based, interactive design tools such as the flight control system design code CONDUIT,[7] the availability of efficient sensitivities can extend interactivity to much larger design problems.

Mathematical Model

The baseline simulation model used in this study is a nonreal-time, blade element-type, coupled rotor–fuselage simulation model.[8] The fuselage is assumed to be rigid and dynamically coupled with the rotor. A total of nine states describe fuselage motion through the nonlinear Euler equations. Fuselage and blades aerodynamics are described through tables of aerodynamic coefficients, and no small angle assumption is required. A coupled flap–lag–torsion elastic rotor model is used.[9] Blades are modeled as Bernoulli–Euler beams. The rotor is discretized using finite elements, with a modal coordinate transformation to reduce the number of degrees of freedom. The elastic deflections are not required to be small. Blade element theory is used to obtain the aerodynamic characteristics on each blade section. Quasi-steady aerodynamics is used, with a three-state dynamic inflow model. No aerodynamic interaction between fuselage, rotor wake, and tail rotor is taken into account.

The helicopter equations of motion are written as a system of nonlinear differential equation in the implicit form $\boldsymbol{f}(\boldsymbol{x}, \dot{\boldsymbol{x}}, \boldsymbol{u}; t) = \boldsymbol{0}$, where t is time. The trim procedure is the same as in Refs. 10 and 11. The rotor equations of motion are transformed into a system of nonlinear algebraic equations using a Galerkin method. The algebraic equations enforcing force and moment equilibrium, the Euler kinematic equations, the inflow equations, and the rotor equations are combined in a single coupled system. The solution yields the harmonics of a Fourier expansion of the rotor degrees of freedom, the pitch control settings, trim attitudes and rates of the entire helicopter, and main and tail rotor inflow.

For the calculation of bandwidth and phase delay according to the "Small Amplitude Attitude Changes" sections of ADS-33,[2] a linearized set of equations of motion is required. These equations are written in the general form

$$\dot{\boldsymbol{x}} = A\boldsymbol{x} + B\boldsymbol{u}, \qquad \boldsymbol{y} = C\boldsymbol{x} + D\boldsymbol{u} \tag{1}$$

and are obtained through a numerical linearization about a trimmed flight condition.

Sensitivity Analysis

The frequency-response matrix corresponding to Eq. (1) is

$$G(i\omega) = C(i\omega I - A)^{-1}B + D \tag{2}$$

and its sensitivity to changes in the generic design parameter p is given by[12]

$$\frac{\partial G(i\omega)}{\partial p} = C(i\omega I - A)^{-1}\frac{\partial A}{\partial p}(i\omega I - A)^{-1} + C(i\omega I - A)^{-1}\frac{\partial B}{\partial p} \tag{3}$$

where it is assumed that C and D do not depend on p. Therefore, the frequency-response matrix $G_{\text{pert}}(i\omega)$ of the system with the perturbed parameter $p + \Delta p$ is given by (to first order)

$$G_{\text{pert}}(i\omega) = G(i\omega) + \frac{\partial G(i\omega)}{\partial p}\Delta p \tag{4}$$

The bandwidth ω_{BW} and phase delay τ_p corresponding to $G_{\text{pert}}(i\omega)$ can then be calculated, and the sensitivities $\partial\omega_{\text{BW}}/\partial p$ and $\partial\tau_p/\partial p$ can be obtained using finite difference approximations.

For the bandwidth specifications, one can define a parameter D as the distance of the point representative of the helicopter from the level 1 boundary on the corresponding ADS-33 specification chart. (See Fig. 1 for an example.) If the point is inside the level 1 region, then the helicopter is likely to be considered "satisfactory without improvement"[2] for a given task, and its Cooper–Harper rating (CHR) will likely between 1 and 3.5, implying that the pilot compensation required will go from none (CHR = 1) to between minimal (CHR = 3) and moderate (CHR = 4).[2]

The distance D is given by

$$D = \sqrt{(x_i - \omega_{\text{BW}})^2 + (y_i - \tau_P)^2} \tag{5}$$

where x_i and y_i are the coordinates of the point of the level 1 boundary curve that is closest to the point representative of the helicopter. The derivative of D with respect to a generic design parameter p is given by

$$\frac{\partial D}{\partial p} = \frac{1}{2D}\left[2(x_i - \omega_{\text{BW}})\left(\frac{\partial x_i}{\partial p} - \frac{\partial \omega_{\text{BW}}}{\partial p}\right) + 2(y_i - \tau_P)\left(\frac{\partial y_i}{\partial p} - \frac{\partial \tau_P}{\partial p}\right)\right] \tag{6}$$

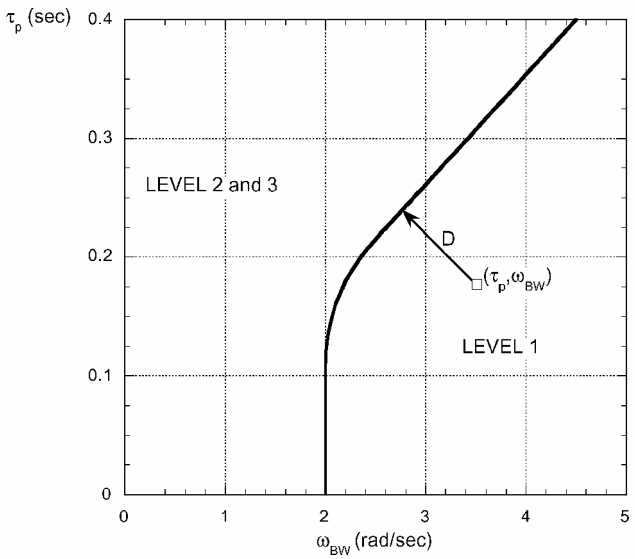

Fig. 1 Definition of the distance from the level 1 boundary.

The derivatives $\partial x_i/\partial p$ and $\partial y_i/\partial p$ can be obtained using finite differences from simple geometric considerations.

The sensitivity $\partial D/\partial p$ describes how the distance from the specification boundary changes when the design parameter p is changed and, therefore, gives a direct indication of how the design parameter affects the satisfaction of the specification. From a computational point of view, it can be observed from the preceding discussion that $\partial D/\partial p$ can be calculated efficiently if the derivatives of the state and control matrices $\partial A/\partial p$ and $\partial B/\partial p$ can also be calculated efficiently, that is, at a fraction of the cost of calculating the baseline A and B matrices. The calculation of $\partial A/\partial p$ and $\partial B/\partial p$ will be discussed next.

The customary linearization process is based on the requirement that the first differential of the equations of motion be equal to zero:

$$\mathrm{d}\boldsymbol{f}(\dot{\boldsymbol{x}}, \boldsymbol{x}, \boldsymbol{u}; t) = 0 \tag{7}$$

Equation (7) can be written as

$$\left[\frac{\partial \boldsymbol{f}}{\partial \boldsymbol{x}}\right]\mathrm{d}\boldsymbol{x} + \left[\frac{\partial \boldsymbol{f}}{\partial \dot{\boldsymbol{x}}}\right]\mathrm{d}\dot{\boldsymbol{x}} + \left[\frac{\partial \boldsymbol{f}}{\partial \boldsymbol{u}}\right]\mathrm{d}\boldsymbol{u} = 0 \tag{8}$$

where the brackets indicate matrices, which are calculated at the trim condition. All three matrices have a number of rows equal to the size of the state vector; the number of columns of the first two is also equal to the size of $\boldsymbol{x}$, whereas the number of columns of the third matrix is equal to the size of $\boldsymbol{u}$. The linearized model is obtained by solving for $\mathrm{d}\dot{\boldsymbol{x}}$:

$$\mathrm{d}\dot{\boldsymbol{x}} = \underbrace{-\left[\frac{\partial \boldsymbol{f}}{\partial \dot{\boldsymbol{x}}}\right]^{-1}\left[\frac{\partial \boldsymbol{f}}{\partial \boldsymbol{x}}\right]}_{\stackrel{\text{def}}{=} A}\mathrm{d}\boldsymbol{x} \underbrace{-\left[\frac{\partial \boldsymbol{f}}{\partial \dot{\boldsymbol{x}}}\right]^{-1}\left[\frac{\partial \boldsymbol{f}}{\partial \boldsymbol{u}}\right]}_{\stackrel{\text{def}}{=} B}\mathrm{d}\boldsymbol{u} \tag{9}$$

which is the first equation of the linearized system, Eq. (1), after dropping the d in the notation for perturbation states and controls. The C and D matrices in Eq. (1) depend on the particular application; in the present work it will be assumed that C is an identity matrix and $D = 0$.

When Eq. (9) is used, the sensitivities of the state and control matrices are given by

$$\frac{\partial A}{\partial p} = \frac{\partial}{\partial p}\left\{-\left[\frac{\partial \boldsymbol{f}}{\partial \dot{\boldsymbol{x}}}\right]^{-1}\left[\frac{\partial \boldsymbol{f}}{\partial \boldsymbol{x}}\right]\right\}$$

$$= \underline{\left[\frac{\partial \boldsymbol{f}}{\partial \dot{\boldsymbol{x}}}\right]^{-1}}\left\{\left[\frac{\partial \boldsymbol{\Delta}}{\partial \dot{\boldsymbol{x}}}\right]\underline{\left[\frac{\partial \boldsymbol{f}}{\partial \dot{\boldsymbol{x}}}\right]^{-1}\left[\frac{\partial \boldsymbol{f}}{\partial \boldsymbol{x}}\right]} - \left[\frac{\partial \boldsymbol{\Delta}}{\partial \boldsymbol{x}}\right]\right\} \tag{10}$$

$$\frac{\partial B}{\partial p} = \frac{\partial}{\partial p}\left\{-\left[\frac{\partial \boldsymbol{f}}{\partial \dot{\boldsymbol{x}}}\right]^{-1}\left[\frac{\partial \boldsymbol{f}}{\partial \boldsymbol{x}}\right]\right\}$$

$$= \underline{\left[\frac{\partial \boldsymbol{f}}{\partial \dot{\boldsymbol{x}}}\right]^{-1}}\left\{\left[\frac{\partial \boldsymbol{\Delta}}{\partial \dot{\boldsymbol{x}}}\right]\underline{\left[\frac{\partial \boldsymbol{f}}{\partial \dot{\boldsymbol{x}}}\right]^{-1}\left[\frac{\partial \boldsymbol{f}}{\partial \boldsymbol{u}}\right]} - \left[\frac{\partial \boldsymbol{\Delta}}{\partial \boldsymbol{x}}\right]\right\} \tag{11}$$

where the underlined terms are already available from the baseline linearization. The vector $\boldsymbol{\Delta}$ is the derivative of the equations of motion of the helicopter with respect to the generic design parameter p, calculated at trim:

$$\boldsymbol{\Delta} = \frac{\partial \boldsymbol{f}}{\partial p} \tag{12}$$

Therefore, the efficient calculation of the sensitivities of bandwidth and phase delay depends on an efficient calculation of $\boldsymbol{\Delta}$ and its derivatives in Eqs. (10) and (11).

The rotor portion of the equations of motion [Eq. (7)] is formulated in a rotating coordinate system. Therefore, the rotor portions of the A and B matrices in Eqs. (9–11) are also formulated in a rotating coordinate system and, in general, will be a function of the blade azimuth angle ψ. A multiblade coordinate transformation (MCT) transforms the rotor portions of A and B into a nonrotating frame. The transformation is performed at a given number of azimuth angles, and the transformed matrices are averaged to remove the residual periodicity, resulting in constant matrices A_{nr} and B_{nr}, respectively. The process can be written in mathematical form as

$$A_{\mathrm{nr}} = \sum_{i=1}^{N_\psi}\left[T^{-1}(\psi_i)A(\psi_i)T(\psi_i) - T^{-1}(\psi_i)\dot{T}(\psi_i)\right] \tag{13}$$

$$B_{\mathrm{nr}} = \sum_{i=1}^{N_\psi} T^{-1}(\psi_i)B(\psi_i) \tag{14}$$

where N_ψ is the number of azimuth angles at which the MCT is performed.

Calculation of the Sensitivities

Bandwidth and phase delay can depend on many rotor, airframe, and flight control system parameters. The derivation of the sensitivities with respect to all of these parameters is beyond the scope of the present study. This paper will describe how to obtain the sensitivities with respect to the rotor blade torsional stiffness GJ. The sensitivities with respect to the blade cross-sectional center of gravity offset x_f, the blade chord c, the area of the horizontal tail S_{HT}, and the gain of the pitch rate feedback to longitudinal cyclic K_q may be found in Ref. 1. Together, these five parameters are representative of a broad class of helicopter design parameters.

A change in torsional stiffness affects both the rotor equations of motion and the Euler rigid-body equations of motion because it changes the structural portion of the rotor equations and the rotor loads, which play the role of forcing functions in the Euler equations. The derivation of the sensitivities of the blade equations will be presented here in detail.

If $\boldsymbol{f}_{MR}$ denotes the portion of the equations of motion $\boldsymbol{f}(\boldsymbol{x}, \dot{\boldsymbol{x}}, \boldsymbol{u}; t) = 0$ corresponding to the rotor equations, it is possible to write

$$\boldsymbol{f}_{MR}(\boldsymbol{x}, \dot{\boldsymbol{x}}, \boldsymbol{u}; t) = \boldsymbol{F}_I(\boldsymbol{x}, \dot{\boldsymbol{x}}, \boldsymbol{u}; t) + \boldsymbol{F}_A(\boldsymbol{x}, \dot{\boldsymbol{x}}, \boldsymbol{u}; t) + \boldsymbol{F}_S(\boldsymbol{x}, \dot{\boldsymbol{x}}, \boldsymbol{u}; t) = \boldsymbol{0} \tag{15}$$

where $\boldsymbol{F}_I$, $\boldsymbol{F}_A$, and $\boldsymbol{F}_S$ are the inertia, aerodynamic, and structural portion of the rotor equations, respectively. Because only $\boldsymbol{F}_S$ is a function of the torsion stiffness, the sensitivity of $\boldsymbol{f}_{MR}$ required in Eq. (12) is given by

$$\frac{\partial \boldsymbol{f}_{MR}}{\partial GJ} = \frac{\partial \boldsymbol{F}_S}{\partial GJ} \tag{16}$$

In the present study, a finite element model of the blade is used, and therefore, the structural portion $\boldsymbol{F}_S$ of the equations of motion is obtained from the assembly of element vectors of nodal structural loads, that is,

$$\boldsymbol{F}_S = \sum_{i=1}^{N_E} \boldsymbol{\Phi}_i \boldsymbol{B}_i \boldsymbol{p}_{Si} \tag{17}$$

where $\boldsymbol{p}_{Si}$ is the structural load vector for the ith finite element, $\boldsymbol{B}_i$ is a matrix that transforms $\boldsymbol{p}_{Si}$ from the local to a global blade coordinate system, $\boldsymbol{\Phi}_i$ is a matrix that performs a modal coordinate transformation to reduce the number of degrees of freedom, and N_E is the number of finite elements used to model the blade. (See Ref. 9 for more details on the entire procedure.)

If the changes with torsion stiffness of the blade normal modes are neglected, then the only term in Eq. (17) that is a functions of GJ is the element load vector $\boldsymbol{p}_{Si}$, and therefore,

$$\frac{\partial \boldsymbol{F}_S}{\partial GJ} = \sum_{i=1}^{N_E} \Phi_i B_i \frac{\partial \boldsymbol{p}_{Si}}{\partial GJ} \tag{18}$$

The structural load vector $\boldsymbol{p}_{Si}$ is given by[9]

$$\boldsymbol{p}_{Si} = \int_0^{l_i} \left\{ \begin{array}{c} M_{l1}\boldsymbol{H}_{v,x}(x_e) + M_{l2}\boldsymbol{H}_{v,xx}(x_e) \\ M_{f1}\boldsymbol{H}_{w,x}(x_e) + M_{f2}\boldsymbol{H}_{w,xx}(x_e) \\ M_{t0}\boldsymbol{H}_{\phi}(x_e) + M_{t1}\boldsymbol{H}_{\phi,x}(x_e) \end{array} \right\} \mathrm{d}x \tag{19}$$

where l_i is the length of the ith finite element and $\boldsymbol{H}_v(x_e)$, $\boldsymbol{H}_w(x_e)$, and $\boldsymbol{H}_{\phi}(x_e)$ are Hermite interpolation polynomials for lag bending, flap bending, and torsion, respectively. Furthermore,[9]

$$M_{t1} = GJ(\phi_{,x} + v_{,xx}w_{,x}) \tag{20}$$

$$M_{t0} = -\tfrac{1}{2}(EI_2 - EI_3)\sin 2\theta_G\left(v_{,xx}^2 - w_{,xx}^2\right) + (EI_2 - EI_3)\cos 2\theta_G(v_{,xx} + 2\phi w_{,xx}) \tag{21}$$

$$M_{f2} = (EI_2 - EI_3)\sin 2\theta_G(v_{,xx} + 2\phi w_{,xx}) + (EI_2 - EI_3)\cos 2\theta_G\phi v_{,xx} + \left(EI_2\sin^2\theta_G + EI_3\cos^2\theta_G\right)w_{,xx} \tag{22}$$

$$M_{f1} = GJ\phi_{,x}v_{,xx} + Tw_{,x} \tag{23}$$

$$M_{l2} = \left(EI_2\cos^2\theta_G + EI_3\sin^2\theta_G\right)v_{,xx} + (EI_2 - EI_3)\sin 2\theta_G(w_{,xx} + 2\phi v_{,xx}) + (EI_2 - EI_3)\cos 2\theta_G\phi w_{,xx} \tag{24}$$

$$M_{l1} = GJ\phi_{,x}w_{,xx} + Tv_{,x} \tag{25}$$

Because only M_{t1}, M_{f1}, and M_{l1} depend on GJ, the sensitivity of the structural load vector is given by

$$\frac{\partial \boldsymbol{p}_{Si}}{\partial GJ} = \int_0^{l_i} \left\{ \begin{array}{c} \dfrac{\partial M_{l1}}{\partial GJ}\boldsymbol{H}_{v,x}(x_e) \\ \dfrac{\partial M_{f1}}{\partial GJ}\boldsymbol{H}_{w,x}(x_e) \\ \dfrac{\partial M_{t1}}{\partial GJ}\boldsymbol{H}_{\phi,x}(x_e) \end{array} \right\} \mathrm{d}x \tag{26}$$

where

$$\frac{\partial M_{t1}}{\partial GJ} = \phi_{,x} + v_{,xx}w_{,x} \tag{27}$$

$$\frac{\partial M_{f1}}{\partial GJ} = \phi_{,x}v_{,xx} \tag{28}$$

$$\frac{\partial M_{l1}}{\partial GJ} = \phi_{,x}w_{,xx} \tag{29}$$

It is clear by examining Eqs. (18) and (26–29) that most of the quantities required for sensitivity calculations are already available as part of the baseline solution and can be reused at no additional cost. The same holds true for the sensitivities of the rotor loads, not described here, which appear in the portion of the equations of motion $\boldsymbol{f}(\boldsymbol{x}, \dot{\boldsymbol{x}}, \boldsymbol{u}; t) = 0$ that contains the Euler rigid-body equations.

The procedure just described can be easily extended to the lag bending stiffness EI_2 and the flap bending stiffness EI_3. All that is needed is to differentiate Eqs. (20–25) with respect to EI_2 or EI_3 instead of GJ and to modify the subsequent equations accordingly. The same is also true for the built-in twist θ_G, except that in this case the changes in the distributed inertia and aerodynamic loads would also need to be considered.

Results

Helicopter Configurations

Two different helicopter configurations are considered in this study, one similar to the Eurocopter BO-105 and the other similar to the Sikorsky UH-60 Blackhawk. For the BO-105, results have been obtained for hover and 40 and 80 kn, with C_T/σ equal to about 0.07. For the UH-60A, results have been obtained for hover and 60 and 120 kn, with $C_T/\sigma = 0.08$. A selection of the most interesting results is presented in this section. Many additional results may be found in Ref. 1.

All of the sensitivities are calculated considering constant variations of the design variable along the blade span. For example, a 10% variation of torsional stiffness of the rotor blade indicates a constant increase along the span of $0.1GJ_{0.75}$. Note that $GJ_{0.75}$ represents the magnitude of the torsional stiffness at the three-quarter radius of the rotor blade. This is only done for simplicity. The procedure can easily accommodate variations of the design variables that change along the blade span. Only some additional bookkeeping modifications are required, but the basic mathematical expressions remain unchanged. All of the UH-60A results were calculated with a small amount of pitch rate feedback.

Sensitivities computed in three different ways will be compared:

1) The first computation used finite difference sensitivities with retrim and mode update. After the baseline calculations, the value of the torsion stiffness GJ is perturbed, and another completely new analysis is performed, including a recalculation of the trim state and of the blade mode shapes. The behavior quantities are calculated for the baseline and the perturbed configuration, and a one-sided, forward finite difference formula is used to obtain the sensitivities.

2) The second computation used finite difference sensitivities without retrim and mode update. This method is the same as the first one, except that the blade normal modes and trim condition are not updated after the perturbation of GJ. The linearized model of the helicopter for the perturbed configuration is obtained by linearizing the equations of motion about the baseline, unperturbed trim condition. This is equivalent to assuming that the equations of motion are linear and, therefore, that the linearized model is independent of the equilibrium position. These results are presented because the semi-analytical method is based on the same assumption, and therefore, they provide a check of the latter results.

3) The last computation used a semi-analytical method. This is the method developed in the present study.

Frequency-Response and Bandwidth Sensitivities

Results for the BO-105 Configuration

Variations of -10 and $+10\%$ of the blade torsional stiffness change the fundamental torsion mode frequency from 3.18 to 3.03 and 3.32/revolution, respectively. The frequency changes for other blade modes are much smaller. Figure 2 shows the value of the sensitivities of pitch bandwidth ω_{BW}, phase delay τ_p, and distance from boundary, D, as a function of the size of the perturbation used in the finite difference calculations. The helicopter is in hover. For all quantities, the semi-analytical values and the finite difference values without retrim and mode update are in excellent agreement for most values of the perturbation size. This validates the derivation of the semi-analytical sensitivities. The semi-analytical sensitivities are almost independent of step size. They are not completely independent because finite difference approximations are still used in some portions of the calculation, and therefore, some truncation error remains for large step sizes. No cancellation errors appear for the smallest step sizes in Fig. 2. The finite difference (FD)-based sensitivities with retrim and updated modes are much more sensitive to step size. Some cancellation errors can be seen for step sizes smaller than 0.01%, large truncation errors for step sizes larger than 1%, and neither cancellation nor truncation errors for step sizes in between. Therefore, the sensitivity can be assumed to be correct for those intermediate values. The relative difference between this and the semi-analytic sensitivity is of about 13%, which, therefore, is the error made in neglecting the changes in trim and blade modes when computing the sensitivities. For all step sizes, the bandwidth is the same as the phase bandwidth, that is, the system is phase limited.

Note that the phase-delay calculations only include effects due to rotor aerodynamics and dynamics and do not take into account real life effects such as actuator delays. The accuracy of the sensitivity calculations does not change, but the absolute values of the delays are 50–100 ms lower than in reality. Because all of the results are

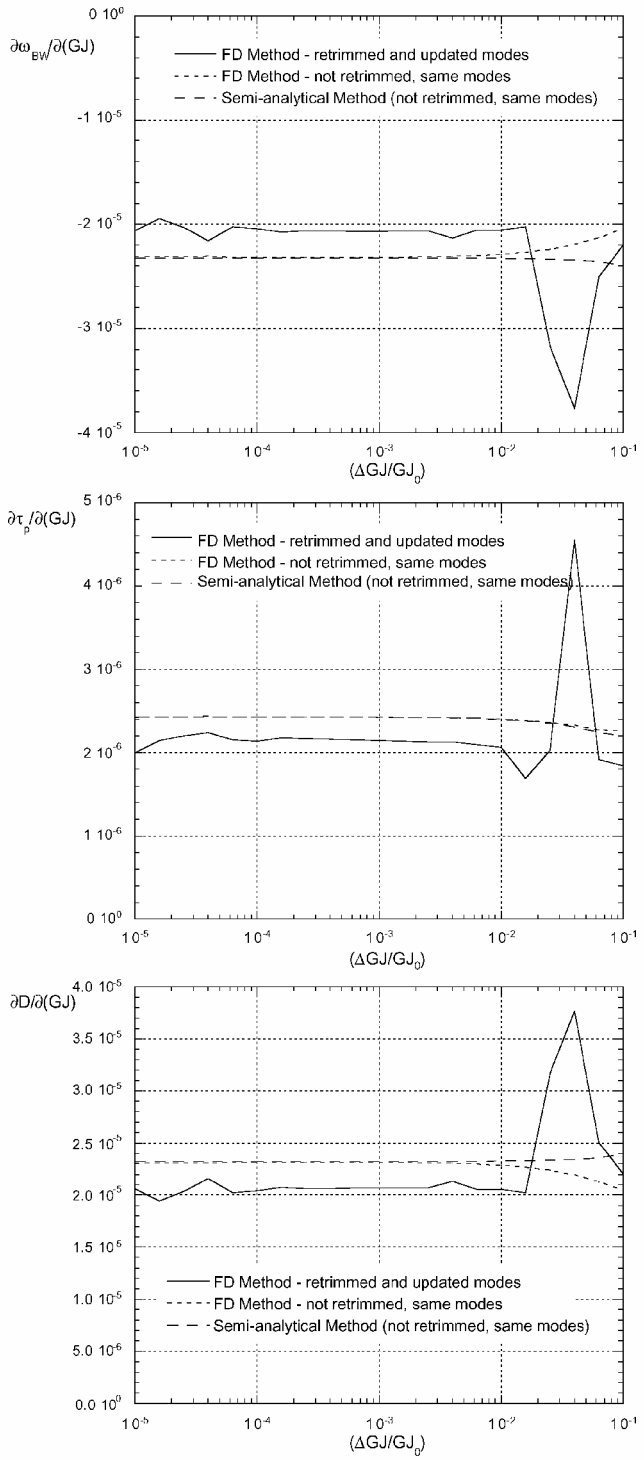

Fig. 2 BO-105 in hover: sensitivity of pitch bandwidth, phase delay, and distance from level 1 boundary with respect to the blade torsional stiffness as a function of the step size of the perturbation.

based on Bode plots, the actuator delays can simply be added to all of the values of τ_p presented subsequently. As to the sensitivities of τ_p, the contribution of the actuators will typically be zero, unless the specific design parameter considered is an actuator design parameter. Therefore, neglecting actuator delays will not affect the sensitivities presented in this section. The same will largely be true for other real life effects such as sensor and computation delays.

Table 1 summarizes the sensitivity results obtained with the three methods. Results for both the pitch and roll axes and for speeds of 0, 40, and 80 kn are presented.

Figure 3 shows bandwidth ω_{BW}, phase delay τ_p, and distance from boundary D, as a function of the blade torsional stiffness GJ, as GJ

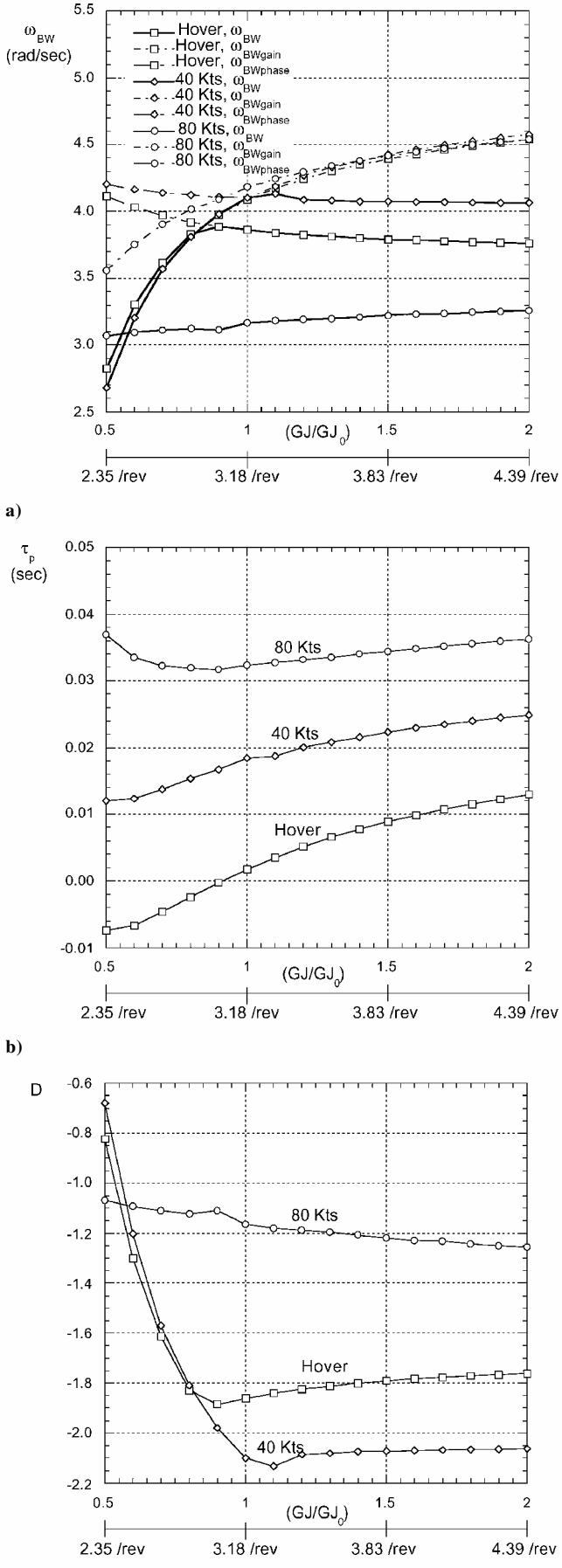

Fig. 3 BO-105: bandwidth ω_{BW}, phase delay τ_p, and distance D from level 1 boundary for small-amplitude attitude changes in pitch as a function of the blade torsional stiffness GJ.

Table 1 BO-105: sensitivities of bandwidth and phase delay with respect to the blade torsional stiffness

Method	Pitch axis			Roll axis		
	$\frac{\partial \tau_p}{\partial GJ}$	$\frac{\partial \omega_{BW}}{\partial GJ}$	$\frac{\partial D}{\partial GJ}$	$\frac{\partial \tau_p}{\partial GJ}$	$\frac{\partial \omega_{BW}}{\partial GJ}$	$\frac{\partial D}{\partial GJ}$
			Hover			
FD retrim	2.15×10^{-6}	-2.07×10^{-5}	2.07×10^{-5}	3.01×10^{-7}	8.44×10^{-5}	3.01×10^{-6}
FD no retrim	2.43×10^{-6}	-2.31×10^{-5}	2.31×10^{-5}	3.67×10^{-7}	8.40×10^{-5}	3.67×10^{-6}
Semi-analytical	2.42×10^{-6}	-2.32×10^{-5}	2.32×10^{-5}	3.68×10^{-7}	8.41×10^{-5}	3.68×10^{-6}
Relative error, %	12.9	12.1	12.1	22.3	−0.381	22.3
			40 kn			
FD retrim	1.47×10^{-6}	-1.10×10^{-5}	-1.23×10^{-4}	2.73×10^{-7}	9.40×10^{-5}	2.73×10^{-6}
FD no retrim	1.81×10^{-6}	-1.34×10^{-5}	-1.30×10^{-4}	3.05×10^{-7}	8.91×10^{-5}	3.05×10^{-6}
Semi-analytical	1.81×10^{-6}	-1.34×10^{-5}	-1.30×10^{-4}	3.06×10^{-7}	8.92×10^{-5}	3.06×10^{-6}
Relative error, %	22.7	21.7	5.63	12.3	−5.18	12.3
			80 kn			
FD retrim	-4.86×10^{-7}	2.24×10^{-5}	-2.24×10^{-5}	3.57×10^{-6}	2.88×10^{-5}	3.57×10^{-5}
FD no retrim	6.63×10^{-7}	1.42×10^{-5}	-1.42×10^{-5}	8.42×10^{-7}	6.96×10^{-5}	8.42×10^{-6}
Semi-analytical	6.61×10^{-7}	1.42×10^{-5}	-1.42×10^{-5}	8.43×10^{-7}	6.97×10^{-5}	8.43×10^{-6}
Relative error, %	−236	−36.5	−36.7	−76.4	142	−76.4

varies from half to twice the baseline value. Recall that ADS-33[2] defines ω_{BW} as the lesser of the gain bandwidth $\omega_{BW_{gain}}$ and the phase bandwidth $\omega_{BW_{phase}}$, and therefore, both types of bandwidth are plotted in Fig. 3. The purpose of Fig. 3 is to help determine whether ω_{BW}, τ_p, and D are linear functions of GJ. If this was the case, then the sensitivities would be constant with GJ, and the values of ω_{BW}, τ_p, and D could be obtained by using simple linear extrapolations. Replacing the actual calculation of a quantity with linear or quadratic extrapolations is a technique commonly used in design optimization and is one of the "approximation concepts"[13] that can greatly increase the computational efficiency of an optimization. Another approximation concept consists of replacing the original optimization problem with a sequence of approximate optimization problems, the solutions of which converge to the solution of the original problem.[13] The approximate problems need to be much faster to solve than the original problem, and the computational gains are obtained by replacing the most expensive calculations for objective function and constraints with, typically, Taylor series approximations. If these approximations are accurate for broad ranges of values of the design variables, they do not need to be recalculated frequently, and the sequence of approximate problems typically converges quickly.

Figure 3 shows that in hover and low-speed flight the bandwidth ω_{BW} is a clearly nonlinear function of GJ for $0.5GJ_0 \leq GJ \leq 2GJ_0$, especially in the neighborhood of the nominal value of GJ. However, most of the nonlinearity is caused by a change of the type of bandwidth that defines ω_{BW}: For low values of GJ, the system is gain limited, that is, $\omega_{BW} = \omega_{BW_{gain}}$, whereas for higher GJ the system is phase limited, that is, $\omega_{BW} = \omega_{BW_{phase}}$. At a speed of 80 kn, the system is always phase limited. Figure 3 shows that the nonlinearity of the individual gain and phase bandwidths is much less pronounced, especially where each represents the entire bandwidth, for example, at hover, $GJ \leq 0.85$ for $\omega_{BW_{gain}}$ and $GJ \geq 0.85$ for $\omega_{BW_{phase}}$. Therefore, a good-quality approximation of ω_{BW} could be obtained by using separate linear Taylor series expansions in GJ for $\omega_{BW_{gain}}$ and for $\omega_{BW_{phase}}$ and then combining the two estimates into ω_{BW}.

Figure 3 shows that the dependency of the phase delay τ_p on GJ is nonlinear, but mildly so, and therefore, linear approximations would be reasonable in most cases. The distance D from the level 1 boundary is a strongly nonlinear function of GJ for hover and low speed, but the nonlinearity comes primarily from the switch from gain- to phase-limited status. Reconstructing D from linear approximations of $\omega_{BW_{gain}}$, $\omega_{BW_{phase}}$, and τ_p is likely to give reasonably accurate values over a broad range of values of GJ, for a very small computational cost.

Figure 3b shows negative values of the phase delay τ_p at hover, for the lower range of values of GJ. These values are physically meaningless and are simply an artifact of applying literally the ADS-33 specification. The specification states that "If phase is nonlinear between ω_{180} and $2\omega_{180}$, τ_p shall be determined from a linear least squares fit to phase curve between ω_{180} and $2\omega_{180}$."[2] Because at hover the phase of the pitch frequency response is indeed nonlinear, because of the presence of a coupled rotor–body mode, τ_p was calculated from the required least-square fit rather than from the actual phase plot, and its value turned out to be negative. ADS-33 does not indicate how to deal with these unphysical values, and no discussion of these issues appears in the literature. Rather than arbitrarily set a course of action, for example, set to zero any negative values of τ_P, it was decided to retain negative values of τ_p in the present study. From the point of view of the proposed methodology, the issue is not very important because all of the sensitivity calculations downstream of the frequency-response perturbations are performed numerically and can be easily modified to accommodate a different procedure to calculate the phase delay τ_p.

Results for the UH-60 Configuration

Figure 4 shows the value of the sensitivities of pitch bandwidth ω_{BW}, phase delay τ_p, and distance from boundary D as a function of the size of the perturbation used in the FD calculations. The helicopter is in hover. As in the case of the BO-105 configuration (Fig. 2), the semi-analytical values and the FD values without retrim and mode update are in excellent agreement for most values of the perturbation size, which validates the derivation of the semi-analytical sensitivities. Again, the semi-analytical sensitivities are almost independent of step size, and no cancellation errors appear for the smallest step sizes in Fig. 4. The FD-based sensitivities with retrim and updated modes are much more sensitive to step size. Some cancellation errors can be seen for step sizes smaller than 0.01%, large truncation errors for step sizes as small as 0.1%, and neither cancellation nor truncation errors for step sizes in between. The relative differences between this and the semi-analytic sensitivity is quite large in relative terms, especially for the bandwidth and, consequently, for the distance from the level 1 boundary. However, the absolute values of these sensitivities are small. In fact, they are between one and two orders of magnitude smaller than the corresponding quantities for the BO-105. In other words, torsional stiffness is a far less important design parameter for bandwidth and phase delay, compared to the BO-105, and therefore, the larger errors made in neglecting changes in trim and mode shapes are less serious. For all step sizes, the bandwidth is the same as the phase bandwidth, that is, the system is phase limited. As in the BO-105 case, actuator delays are not included in the calculations. Table 2 summarizes the sensitivity results obtained with the three methods for both the pitch and roll axes and for speeds of 0, 60, and 120 kn.

Figure 5 shows bandwidth ω_{BW}, phase delay τ_p, and distance from boundary, D, as a function of the blade torsional stiffness GJ, as GJ varies from half to twice the baseline value. Both the gain bandwidth $\omega_{BW_{gain}}$ and the phase bandwidth $\omega_{BW_{phase}}$ are plotted in Fig. 5. As for Fig. 3, the purpose of Fig. 5 is to help determine

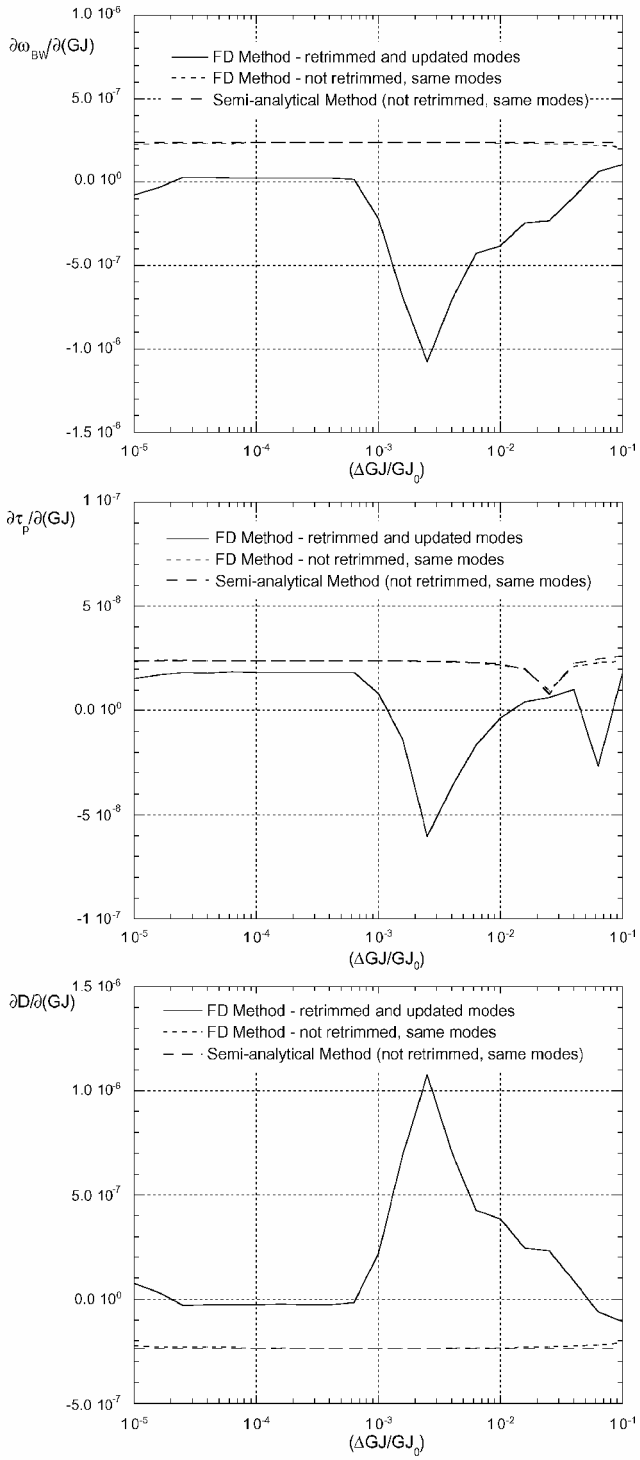

Fig. 4 UH-60A in hover: sensitivity of pitch bandwidth, phase delay, and distance from level 1 boundary with respect to the blade torsional stiffness as a function of the step size of the perturbation.

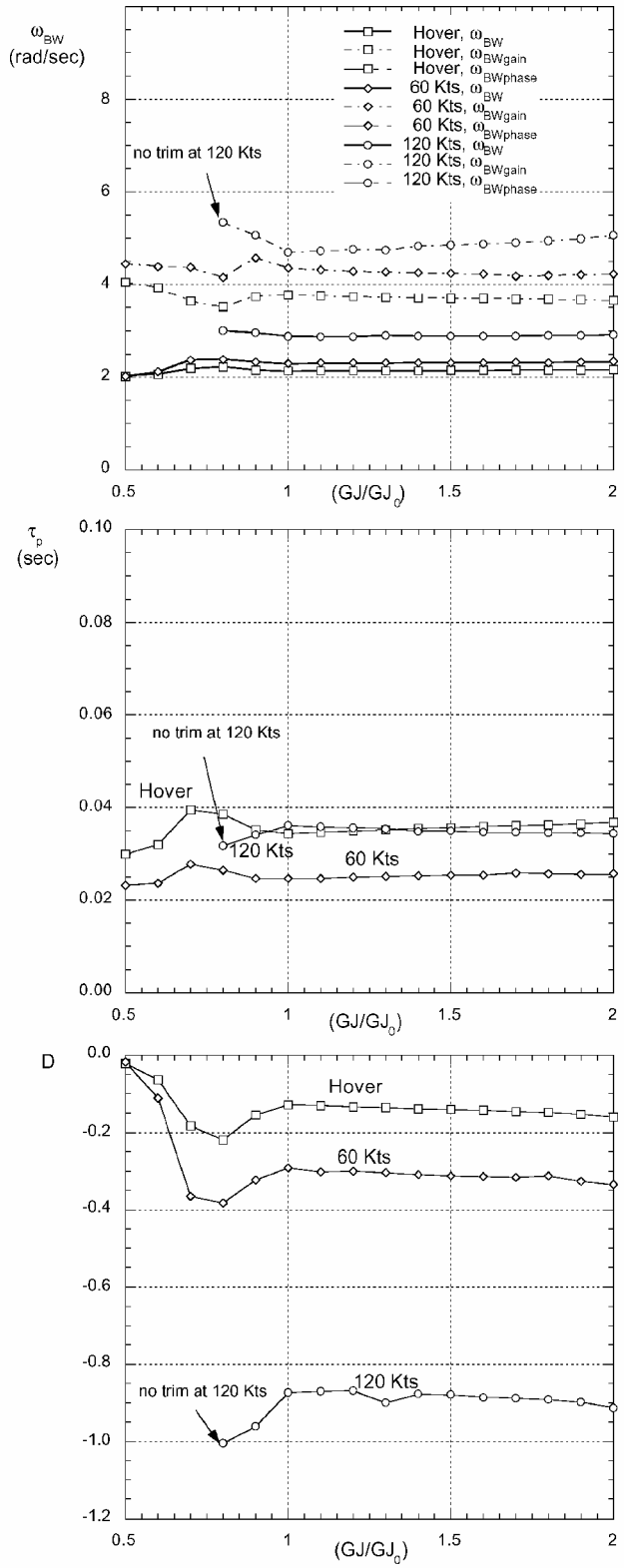

Fig. 5 UH-60A: bandwidth, phase delay, and distance *D* from level 1 boundary for small-amplitude attitude changes in pitch as a function of the blade torsional stiffness *GJ*.

whether ω_{BW}, τ_p, and D are linear functions of GJ. For torsion stiffnesses greater than the baseline, ω_{BW}, τ_p, and D change very little with GJ, and linear extrapolations will be accurate. For values of GJ smaller than the baseline, the phase bandwidth is also almost constant. The gain bandwidth is slightly more nonlinear with GJ, but $\omega_{\mathrm{BW}} = \omega_{\mathrm{BW_{phase}}}$ for all of the values of GJ and speed considered, so that $\omega_{\mathrm{BW_{gain}}}$ never comes into play.

The phase delay τ_p on GJ is also essentially constant for $GJ \geq GJ_0$ and somewhat nonlinear for $GJ \leq GJ_0$. In the latter case, a linear approximation would be adequate as long as the perturbations of GJ are no greater than 0.2–0.3GJ_0. Limiting the design changes from one iteration to the next is a typical technique in design optimization, called "move limits," especially when approximation concepts are used.[13] Therefore, with move limits of 20–30% of the baseline torsion stiffness when $GJ \leq GJ_0$, it should be possible to use linear approximations to τ_p. The distance D from the level 1 boundary is a more nonlinear function of GJ than ω_{BW} and τ_p, as shown in Fig. 5, but it can still be computed accurately and inexpensively from linear approximations to ω_{BW} and τ_p over a broad range of values of GJ.

Table 2 UH-60A: sensitivities of bandwidth and phase delay with respect to the blade torsional stiffness

Method	Pitch axis			Roll axis		
	$\frac{\partial \tau_p}{\partial GJ}$	$\frac{\partial \omega_{BW}}{\partial GJ}$	$\frac{\partial D}{\partial GJ}$	$\frac{\partial \tau_p}{\partial GJ}$	$\frac{\partial \omega_{BW}}{\partial GJ}$	$\frac{\partial D}{\partial GJ}$
			Hover			
FD retrim	1.84×10^{-8}	2.57×10^{-8}	-2.57×10^{-8}	-1.39×10^{-8}	1.77×10^{-6}	-1.39×10^{-7}
FD no retrim	2.39×10^{-8}	2.37×10^{-7}	-2.37×10^{-7}	9.35×10^{-9}	1.98×10^{-6}	9.35×10^{-8}
Semi-analytical	2.39×10^{-8}	2.36×10^{-7}	-2.36×10^{-7}	9.41×10^{-9}	1.97×10^{-6}	9.41×10^{-8}
Relative error, %	30.0	821	820	−168	11.8	−168
			60 kn			
FD retrim	1.52×10^{-8}	8.79×10^{-8}	-8.78×10^{-8}	2.57×10^{-9}	2.35×10^{-6}	2.57×10^{-8}
FD no retrim	1.63×10^{-8}	3.97×10^{-7}	-3.97×10^{-7}	1.58×10^{-8}	2.58×10^{-6}	1.58×10^{-7}
Semi-analytical	1.63×10^{-8}	3.96×10^{-7}	-3.96×10^{-7}	1.56×10^{-8}	2.57×10^{-6}	1.56×10^{-7}
Relative error, %	6.86	350	350	506	9.34	506
			120 kn			
FD retrim	-2.61×10^{-8}	-2.70×10^{-7}	2.70×10^{-7}	-1.18×10^{-8}	2.31×10^{-6}	-2.31×10^{-6}
FD no retrim	-8.13×10^{-4}	1.95×10^{-7}	-1.95×10^{-7}	-4.92×10^{-9}	2.16×10^{-6}	-2.16×10^{-6}
Semi-analytical	-8.15×10^{-4}	1.92×10^{-7}	-1.92×10^{-7}	-4.94×10^{-9}	2.17×10^{-6}	-2.17×10^{-6}
Relative error, %	3.12×10^{6}	−171	−171	−58.1	−60.7	−60.7

Table 3 BO-105 in hover: natural frequency ω and damping ratio ζ variations for a 10% increase of torsional stiffness, exact and linearly extrapolated results

	ω, /revolution				ζ			
		$\Delta GJ = +10\%$		Relative		$\Delta GJ = +10\%$		Relative
N	Baseline	Exact	Extrapolated	error, %	Baseline	Exact	Extrapolated	error, %
1	5.5290	5.5284	5.5285	0.00	0.0160	0.0160	0.0160	−0.11
2	4.4900	4.4894	4.4895	0.00	0.0193	0.0193	0.0193	−0.11
3	4.4814	4.4806	4.4807	0.00	0.0194	0.0193	0.0193	−0.14
4	4.4314	4.4557	4.4538	−0.04	0.0685	0.0665	0.0664	−0.04
5	4.0608	4.1773	4.1830	0.14	0.0862	0.0863	0.0863	0.01
6	3.5015	3.5008	3.5009	0.00	0.0250	0.0250	0.0250	−0.13
7	3.4426	3.4653	3.4632	−0.06	0.0877	0.0850	0.0850	0.00
8	3.4319	3.4564	3.4544	−0.06	0.0877	0.0847	0.0846	−0.06
9	3.0624	3.1810	3.1869	0.18	0.1154	0.1145	0.1145	−0.02
10	3.0586	3.1759	3.1819	0.19	0.1169	0.1162	0.1161	−0.10
11	2.4392	2.4630	2.4609	−0.09	0.1242	0.1201	0.1201	0.00
12	2.0736	2.1900	2.1958	0.26	0.1624	0.1589	0.1589	−0.02
13	2.0019	2.0007	2.0036	0.15	0.1609	0.1641	0.1639	−0.16
14	1.8419	1.8443	1.8435	−0.05	0.0601	0.0561	0.0558	−0.49
15	1.0973	1.0963	1.0984	0.19	0.3456	0.3496	0.3481	−0.41
16	1.0508	1.0481	1.0512	0.29	0.2998	0.3062	0.3056	−0.18
17	1.0246	1.0247	1.0246	−0.01	1.0000	1.0000	1.0000	0.00
18	0.9755	0.9716	0.9743	−0.28	0.9978	0.9978	0.9980	0.01
19	0.7858	0.7891	0.7900	−0.11	0.1715	0.1616	0.1605	−0.71
20	0.7162	0.7177	0.7183	−0.09	0.1512	0.1429	0.1422	−0.46
21	0.4403	0.4389	0.4376	−0.29	1.0000	1.0000	1.0000	0.00
22	0.3002	0.2961	0.2962	0.05	0.4387	0.4374	0.4366	−0.19
23	0.2592	0.2598	0.2604	0.22	0.1957	0.1860	0.1861	0.05
24	0.1351	0.1354	0.1354	−0.03	0.5504	0.5667	0.5664	−0.07
25	0.0145	0.0146	0.0146	−0.04	0.2751	0.2684	0.2683	−0.02
26	0.0119	0.0120	0.0120	−0.04	−0.3484	−0.3425	−0.3423	−0.07
27	0.0099	0.0099	0.0099	−0.14	1.0000	1.0000	1.0000	0.00
28	0.0062	0.0062	0.0062	−0.06	1.0000	1.0000	1.0000	0.00

Pole Position Sensitivities

This section show results concerning the location of the poles, or stability eigenvalues, of the helicopter. ADS-33 contains criteria for the position of the rigid-body poles in its midterm response to control input section, Paragraph 3.3.2.1.[2] The study of helicopter poles is obviously also important for aeromechanic analyses, where rotor stability is addressed. The poles are the eigenvalues of the state matrix $\boldsymbol{A}(p)$. After a perturbation Δp, the new poles are the eigenvalues of the new matrix $\boldsymbol{A}(p + \Delta p)$:

$$\boldsymbol{A}(p + \Delta p) = \boldsymbol{A}(p) + \sum_{k=1}^{\infty} \frac{1}{k!} \frac{\mathrm{d}^k \boldsymbol{A}}{\mathrm{d}p^k} \Delta p^k \approx \boldsymbol{A}(p) + \frac{\mathrm{d}\boldsymbol{A}}{\mathrm{d}p} \Delta p \quad (30)$$

after truncating the Taylor series expansion at the linear term. The derivative $\mathrm{d}\boldsymbol{A}/\mathrm{d}p$ in Eq. (30) is given by

$$\frac{\mathrm{d}\boldsymbol{A}}{\mathrm{d}p} = \frac{\partial \boldsymbol{A}}{\partial \boldsymbol{x}_{\mathrm{trim}}} \frac{\partial \boldsymbol{x}_{\mathrm{trim}}}{\partial p} + \frac{\partial \boldsymbol{A}}{\partial \boldsymbol{\Phi}} \frac{\partial \boldsymbol{\Phi}}{\partial p} + \frac{\partial \boldsymbol{A}}{\partial p} \approx \frac{\partial \boldsymbol{A}}{\partial p} \quad (31)$$

after neglecting the changes of $\boldsymbol{A}$ due to changes of mode shapes and trim conditions. ($\boldsymbol{\Phi}$ and $\boldsymbol{x}_{\mathrm{trim}}$ are the matrix of blade mode shapes and the vector of trim variables, respectively.)

Two types of eigenvalues will be compared in this section. The first consists of the eigenvalues of the perturbed matrix $\boldsymbol{A}(p + \Delta p)$, which also include the effect of trim and mode shape changes. These will be considered the exact eigenvalues. The second consists of the eigenvalues of an approximate perturbed matrix $\boldsymbol{A}$, obtained from the truncated linear Taylor series expansion of Eq. (30), with the approximation of Eq. (31), that is, with the changes of trim and mode shapes neglected. These will be called the linearly extrapolated eigenvalues.

Table 3 contains information on the undamped natural frequency ω and the damping ratio ζ for all of the real and complex-conjugate

Table 4 UH-60A in hover: pole natural frequency and damping variations for a 10% increase of torsional stiffness, exact and linearly extrapolated results

	ω, /revolution				ζ			
		$\Delta GJ = +10\%$		Relative		$\Delta GJ = +10\%$		Relative
N	Baseline	Exact	Extrapolation	error, %	Baseline	Exact	Extrapolation	error, %
1	6.2965	6.5272	6.5223	−0.08	0.0888	0.0894	0.0902	−0.84
2	6.0482	6.0613	6.0647	0.06	0.2611	0.2566	0.2578	0.44
3	5.2982	5.5322	5.5270	−0.09	0.1075	0.1073	0.1065	−0.70
4	5.2938	5.5228	5.5173	−0.10	0.1050	0.1062	0.1054	−0.78
5	5.1874	5.1981	5.2023	0.08	0.3056	0.3003	0.3014	0.37
6	5.0547	5.0613	5.0657	0.09	0.3516	0.3470	0.3481	0.32
7	4.3522	4.5538	4.5492	−0.10	0.4681	0.1278	0.1268	−0.83
8	4.3249	4.3540	4.3593	0.12	0.1294	0.4649	0.4657	0.16
9	3.8309	3.8373	3.8416	0.11	0.0877	0.0881	0.0876	−0.67
10	2.8471	2.8537	2.8581	0.15	0.1200	0.1207	0.1196	−0.85
11	2.8331	2.8398	2.8442	0.15	0.1195	0.1201	0.1192	−0.76
12	1.8472	1.8532	1.8576	0.23	0.1806	0.1818	0.1803	−0.82
13	1.8377	1.8482	1.8450	−0.17	0.2246	0.2237	0.2225	−0.56
14	1.4990	1.4991	1.4992	0.00	1.0000	1.0000	1.0000	0.00
15	1.4094	1.4090	1.4091	0.00	0.1863	0.1825	0.1849	1.32
16	1.2268	1.2140	1.2146	0.04	0.9847	0.9861	0.9857	−0.04
17	0.9891	0.9971	0.9931	−0.39	0.4972	0.4893	0.4893	−0.01
18	0.8985	0.9082	0.9053	−0.32	0.4442	0.4421	0.4395	−0.59
19	0.7546	0.7546	0.7548	0.03	0.2472	0.2439	0.2460	0.85
20	0.6762	0.6527	0.6621	1.43	1.0000	1.0000	1.0000	0.00
21	0.2743	0.2726	0.2735	0.32	0.9905	0.9819	0.9868	0.50
22	0.2663	0.2658	0.2660	0.09	0.8018	0.7915	0.7977	0.78
23	0.2002	0.1999	0.2005	0.29	0.6027	0.5954	0.5954	−0.01
24	0.1388	0.1401	0.1393	−0.57	0.8280	0.8309	0.8270	−0.47
25	0.0224	0.0223	0.0224	0.30	−0.0219	−0.0229	−0.0226	−1.47
26	0.0122	0.0122	0.0121	−0.15	0.9252	0.9260	0.9262	0.02
27	0.0090	0.0090	0.0090	−0.25	−1.0000	−1.0000	−1.0000	0.00
28	0.0072	0.0072	0.0071	−0.28	1.0000	1.0000	1.0000	0.00

poles of the BO-105-like configuration in hover. For each pole, Table 3 lists baseline value of ω and ζ; the exact values following a perturbation of blade torsional stiffness ΔGJ equal to 10% of the baseline value; the values extrapolated using a first-order Taylor series expansion in terms of GJ, with the gradients obtained using the semi-analytical method of this paper and no retrim or update of blade normal modes; and the relative error between the exact and the extrapolated values. Table 3 clearly shows that the extrapolated values are in excellent agreement with the exact values. The maximum relative errors for the damping ratio ζ and the natural frequency ω are, respectively, 0.71 and 0.29% in absolute value. The agreement is also excellent for $\Delta GJ = \pm 20\%$, for $V = 40$ kn, and both $\Delta GJ = \pm 10$ and $\pm 20\%$ (Ref. 1) and very good for $V = 80$ kn and both $\Delta GJ = \pm 10$ and $\pm 20\%$ (Ref. 1).

Table 4 contains the same type of information as Table 3 but for the UH-60-like configuration. The agreement between the exact and the extrapolated perturbed eigenvalues is very good, with a maximum relative error for ω and ζ of less than 1.5% in absolute value. Similarly good results are obtained for $\Delta GJ = \pm 20\%$ and at speeds of 60 and 120 kn for both $\Delta GJ = \pm 10$ and $\pm 20\%$ (Ref. 1).

Computational Efficiency

With the semi-analytical method described in the paper, the additional cost required to obtain the sensitivities of bandwidth, phase delay, and poles with respect to the torsion stiffness GJ is 4% of the cost of one full linearized analysis. In other words, if an FD-based calculation of the sensitivities requires 2 linearized analyses (assuming single-sided FDs), then semi-analytical sensitivities require the equivalent of 1.04 analyses. This cost is essentially independent of flight condition or helicopter configuration because the steps required for the semi-analytical calculations are exactly the same, and none of them contains iterative procedures.

The semi-analytic sensitivities are essentially independent of perturbation step size. Therefore, they do not require a preliminary determination of appropriate values of the step size, which would be advisable for FD-based calculations. This will usually result in additional computational efficiency.

In the present study, only one value of GJ was used. In a more realistic design situation, a spanwise distribution of GJ would be desired, and this distribution would be defined by giving the values of GJ at several spanwise stations. Then, the sensitivity with respect to GJ would actually be composed of the sensitivities with respect to each of the values of GJ. In this case, the computational cost of the sensitivities will scale linearly with the number of spanwise stations: For GJ defined at n spanwise stations, the FD-based sensitivities will require $n + 1$ linearizations, assuming one-sided differences, whereas the semi-analytical method will require at most the equivalent of $1 + 0.04n$ linearizations. In fact, it should be possible to reduce the computational cost even further by exploiting the fact that most of the sensitivities of the structural load vectors, Eq. (26), will usually be zero. For example, if GJ is defined at N_E spanwise stations, one for each finite element used to model the blade, and if it is assumed that GJ is constant over each element, then in the summation of Eq. (18) only one term will be nonzero, and the calculation of the sensitivities with respect to all of the values of GJ will have a total additional cost of 4% of one full linearized analysis. In any case, it is clear that the computational gains will increase quickly with problem size.

In the present study, only sensitivities with respect to the torsion stiffness GJ were considered. However, it is easy to see that the same computational gains could be obtained for the sensitivities with respect to the flap bending stiffness EI_2 and the lag bending stiffness EI_3. In fact, the only difference is that expressions equivalent to those of Eqs. (27–29) would have to be obtained by taking derivatives of Eqs. (20–25) with respect to EI_2 and EI_3. The rest of the semi-analytical procedure would remain unchanged. To some extent, the same is also true for the built-in twist, which is part of the total geometric pitch angle θ_G. However, θ_G appears not only in the structural portion of the equation but also in the inertia and in the aerodynamic portions of Eq. (15), and these portions would have to be considered as well.

Finally, the trim calculations also play a role in the computational efficiency of the sensitivity calculations. The trim procedure[11] used in the present study requires the iterative solution of a system of

nonlinear algebraic equations. For the 46 design variables used in this study, the trim solution usually requires 50–55 function evaluations if the initial trim guess is good (otherwise, up to two or three times as many). Each function evaluation requires the calculation of aerodynamic, structural, and inertia loads at a given number of azimuth angles, depending on the required accuracy, and therefore, its cost is comparable to that of the derivation of one column of the state matrix or the control matrix. As a consequence, the computational cost of trimming the helicopter is comparable to that of one linearized analysis if the initial trim guess is good and to two to three linearized analyses otherwise. The semi-analytical sensitivities neglect the changes in trim and normal modes and, therefore, do not require retrimming. In Ref. 14, results are reported of an optimization study conducted with semi-analytical and FD-based sensitivities, in which using the former leads to the same optimum designs as with the latter (and with substantially greater efficiency). Therefore, it seems reasonable to assume that trim and normal mode updates can be neglected in the calculation of the sensitivities. This is automatically done for the semi-analytical sensitivities, but can also be done with FD-based sensitivities, and speed up somewhat the calculation of the latter.

Conclusions

This paper describes an efficient technique to calculate the sensitivities of bandwidth, phase delay, and poles with respect to a rotor blade structural parameter, namely, the torsion stiffness GJ. Bandwidth and phase delay are defined according to the ADS-33 handling qualities specification. The poles can be used to evaluate the handling qualities of the helicopter, again according to ADS-33, and to evaluate its aeromechanic stability. The technique is based on the derivation of expressions for the sensitivities using chain rule differentiation of appropriate portions of the equations of motion. An examination of the resulting expressions indicates that the portions most expensive to calculate are already available as part of the baseline calculations and can, therefore, be reused as part of the sensitivity calculations at no additional cost. Two configurations were studied, namely, a hingeless rotor configuration similar to the Eurocopter BO-105 and an articulated rotor configuration similar to the Sikorsky UH-60.

The main results of the study follow:

1) The semi-analytical sensitivities are in excellent agreement with the corresponding FD-based sensitivities computed by neglecting changes in trim and blade normal modes due to changes in design parameters. The semi-analytical sensitivities are not completely independent from step size because FD approximations are still used in some portions of the calculations, but they are far less sensitive to step size than FD-based sensitivities.

2) For the hingeless rotor configuration, phase bandwidth, gain bandwidth, phase delay, and poles are only weakly nonlinear functions of the torsion stiffness GJ, and therefore, linear approximations based on truncated Taylor series expansions in terms of GJ are accurate for broad variations of GJ. The same is mostly true for the articulated rotor configuration. Here, however, move limits are recommended for linear approximations to the phase delay for low values of GJ.

3) The new technique is computationally very efficient. The additional cost of calculating the sensitivities with respect to GJ is 4% of that of a complete linearized analysis, regardless of rotor configuration and flight speed. For multiple values of GJ, as would be needed to define a spanwise distribution, the cost of each sensitivity is at most 4% of a linearized analysis. The figure is expected to apply also to sensitivities with respect to flap and lag stiffness.

Acknowledgments

This research was supported by the National Rotorcraft Technology Center under the Rotorcraft Center of Excellence Program, Technical Monitor Yung Yu. This is a revised version of a paper presented at the 57th Annual Forum of the American Helicopter Society, Washington D.C., 9–11 May 2001.

References

[1] Fusato, D., "Design Sensitivity Analysis and Optimization for Helicopter Handling Qualities Improvement," Ph.D. Dissertation, Dept. of Aerospace Engineering, Univ. of Maryland, College Park, MD, May 2002.

[2] "Aeronautical Design Standard, Performance Specification, Handling Qualities Requirements for Military Rotorcraft," U.S. Army Aviation and Missile Command, ADS-33E-PRF, Redstone Arsenal, AL, March 2000.

[3] Haftka, R. T., and Gürdal, Z., *Elements of Structural Optimization*, 3rd ed., Kluwer Academic, Norwell, MA, 1991.

[4] Sahasrabudhe, V., and Celi, R., "Efficient Treatment of Moderate Amplitude Constraints for Handling Qualities Design Optimization," *Journal of Aircraft*, Vol. 34, No. 6, 1997, pp. 730–739.

[5] Sahasrabudhe, V., Celi, R., and Tits, A., "Integrated Rotor-Flight Control System Optimization with Aeroelastic and Handling Qualities Constraints," *Journal of Guidance, Control, and Dynamics*, Vol. 20, No. 2, 1997, pp. 217–225.

[6] Celi, R., "Recent Applications of Design Optimization to Rotorcraft: A Survey," *Journal of Aircraft*, Vol. 36, No. 1, 1999, pp. 176–189.

[7] Tischler, M. B., Colbourne, J. D., Morel, M. R., Biezad, D. J., Levine, W. S., and Moldoveanu, V., "CONDUIT—A New Multidisciplinary Integration Environment for Flight Control Development," AIAA Guidance, Navigation, and Control Conf., Aug. 1997.

[8] Theodore, C., and Celi, R., "Helicopter Flight Dynamic Simulation with Refined Aerodynamic and Flexible Blade Modeling," *Journal of Aircraft*, Vol. 39. No. 4, 2002, pp. 577–586.

[9] Celi, R., "Helicopter Rotor Blade Aeroelasticity in Forward Flight with an Implicit Structural Formulation," *AIAA Journal*, Vol. 30, No. 9, 1992, pp. 2274–2282.

[10] Chen, R. T. N., and Jeske, J. A., "Kinematic Properties of the Helicopter in Coordinated Turns," NASA TP 1773, April 1981.

[11] Celi, R., "Hingeless Rotor Dynamics in Coordinated Turns," *Journal of the American Helicopter Society*, Vol. 36, No. 4, 1991, pp. 39–47.

[12] Jones, C., and Celi, R., "Frequency Response Sensitivity Functions for Helicopter Frequency Domain System Identification," *Journal of the American Helicopter Society*, Vol. 42, No. 3, 1997, pp. 244–253.

[13] Schmit, L. A., "Structural Synthesis: Its Genesis and Development," *AIAA Journal*, Vol. 19, No. 10, 1981, pp. 1249–1263.

[14] Fusato, D., and Celi, R., "Multidisciplinary Design Optimization for Aeromechanics and Handling Qualities," Twenty-Eighth European Rotorcraft Forum, Paper 2, Sept. 2002.